Chemistry & Biology
Article

Discovery and Characterization of a Cell-Permeable, Small-Molecule c-Abl Kinase Activator that Binds to the Myristoyl Binding Site

Jingsong Yang,[1,*] Nino Campobasso,[2] Mangatt P. Biju,[1] Kelly Fisher,[1] Xiao-Qing Pan,[1] Josh Cottom,[2] Sarah Galbraith,[1] Thau Ho,[2] Hong Zhang,[2] Xuan Hong,[2] Paris Ward,[2] Glenn Hofmann,[2] Brett Siegfried,[2] Francesca Zappacosta,[2] Yoshiaki Washio,[2] Ping Cao,[2] Junya Qu,[2] Sophie Bertrand,[2] Da-Yuan Wang,[2] Martha S Head,[2] Hu Li,[2] Sheri Moores,[1] Zhihong Lai,[1] Kyung Johanson,[2] George Burton,[2] Connie Erickson-Miller,[1] Graham Simpson,[2] Peter Tummino,[1] Robert A. Copeland,[1] and Allen Oliff[1,2]
[1]Oncology Research and Development
[2]Platform Technology and Science
GlaxoSmithKline, 1250 South Collegeville Road, Collegeville, PA 19426, USA
*Correspondence: jingsong.2.yang@gsk.com
DOI 10.1016/j.chembiol.2010.12.013

SUMMARY

c-Abl kinase activity is regulated by a unique mechanism involving the formation of an autoinhibited conformation in which the N-terminal myristoyl group binds intramolecularly to the myristoyl binding site on the kinase domain and induces the bending of the αI helix that creates a docking surface for the SH2 domain. Here, we report a small-molecule c-Abl activator, DPH, that displays potent enzymatic and cellular activity in stimulating c-Abl activation. Structural analyses indicate that DPH binds to the myristoyl binding site and prevents the formation of the bent conformation of the αI helix through steric hindrance, a mode of action distinct from the previously identified allosteric c-Abl inhibitor, GNF-2, that also binds to the myristoyl binding site. DPH represents the first cell-permeable, small-molecule tool compound for c-Abl activation.

INTRODUCTION

Protein kinases are a key group of regulators of biological processes, particularly the signal transduction pathways. Consequently, the regulation of kinase activities constitutes an essential element in maintaining normal cellular functions. The activity of protein kinases can be modulated through several mechanisms such as subcellular localization, interaction with accessory proteins and ligands, and phosphorylation/dephosphorylation. One common mechanism of kinase activation is the conformational reorganization of the activation loop located between the N- and C-lobes of the kinase domain. This conformational change is prompted by phosphorylation of key residue(s) on/near the activation loop. Additionally, global conformational changes and/or reorganization of the domain structures can also contribute to kinase activation.

In the area of kinase regulation, c-Abl kinase serves as an example of how conformational changes, coupled with protein phosphorylation, modulate its kinase activity. c-Abl is a nonreceptor tyrosine kinase that shares sequence homology with the Src kinase family (Wang, 1993). Like other members of the Src family, the N-terminal portion of c-Abl is composed of three Src homology domains (SH1/catalytic, SH2, and SH3 domains). c-Abl also contains a unique N-terminal cap (~80 amino acids) that plays an important role in the regulation of its kinase activity. The C-terminal portion of c-Abl is composed of an array of signaling and recognition domains that are involved in specific cellular functions of c-Abl, including a DNA-binding domain, an actin-binding domain, several docking sites for partner proteins, and nuclear localization/export signals. c-Abl localizes to both the nucleus and cytoplasm. Evidence suggests that nuclear c-Abl is involved in cell-cycle regulation and stress responses to DNA damage, oxidation, and ionization whereas cytoplasmic c-Abl plays a role in morphogenesis, F-actin dynamics, and signal transduction induced by extracellular stimuli (Taagepera et al., 1998; Wang, 1993; Van Etten, 1999; Sirvent et al., 2008). There are two human c-Abl isoforms, c-Abl 1a and 1b, derived from alternative splicing events (Shtivelman et al., 1986). They differ only in the N-terminal cap region. c-Abl 1b is 19 amino acids longer and is myristoylated on the N-terminal glycine, whereas c-Abl 1a is not myristoylated. This difference has important implications in the regulation of the c-Abl kinase activity.

c-Abl is normally maintained in its inactive state in the cell. Over the years, its mechanism of regulation remained largely unknown. Although its N-terminal region shares significant homology with the Src family kinases, it does not contain the C-terminal tyrosine that plays an essential role in the regulation of Src kinase activity (Xu et al., 1997; Williams et al., 1997). Recently, crystal structures of the N-terminal portion of c-Abl 1b have been resolved that shed light on the potential regulatory mechanism of this enzyme (Nagar et al., 2003, 2006). This portion of c-Abl contains minimally required components for the proper regulation of the kinase activity. Based on the structural data, it was proposed that the c-Abl kinase activity is inhibited through the formation of an assembled conformation (Figure 1). In this state, the N-terminal myristoyl group binds to a deep and largely hydrophobic pocket, often called the

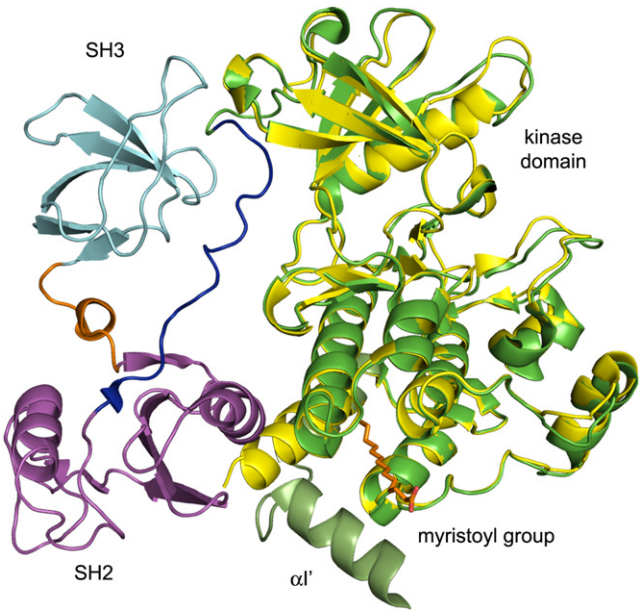

Figure 1. Autoinhibited, Assembled c-Abl Structure (PDB code: 1OPK) with a Myristoyl Group

Helix αI′ is highlighted in smudge green. An overlay of the c-Abl kinase domain only structure (PDB code: 1M52) is colored yellow to highlight difference in respective αI helixes with and without SH2 and N-terminal myristoyl.

myristoyl binding site, on the C-lobe of the kinase domain. This binding helps form a compact conformation in which the SH2 domain docks onto the kinase domain and the SH3 domain interacts with both the kinase domain and the linker between the SH2 and the kinase domain. In this compact conformation, the structural plasticity of the N- and C-lobes required for catalysis is restricted and the enzyme is in an autoinhibited state.

One key feature of this mechanism is the bending of the αI helix on the C-lobe of the kinase domain induced by N-terminal myristoyl binding to the myristoyl binding site. The bending of the αI helix starts at Phe516 and is followed by a short loop and concluded by a new three-turn helix, called the αI' helix (Figure 1). This sharp bend of the αI helix is required to form a docking surface for the SH2 domain. When the myristoyl group is dislodged from the myristoyl binding site, the αI helix then adopts an extended and straight conformation (Figure 1) which clashes with the SH2 domain and prevents its docking onto the kinase domain (Nagar et al., 2003). The resulting open conformation has an elongated shape with the SH2 domain residing on top of the N-lobe of the kinase domain and the SH3 domain completely dissociated from the kinase domain (Nagar et al., 2006). c-Abl kinase in this open conformation has elevated kinase activity (partial activation) which triggers the autoactivation cycle by phosphorylating Y412 on the activation loop and Y245 in the linker between the SH2 and the kinase domains. Full activation of c-Abl is achieved following the phosphorylation of these two key tyrosine residues (Brasher and Van Etten, 2000). Various pieces of evidence support this model of c-Abl activation. For example, mutations in the SH2 and SH3 domains that could potentially disrupt domain interactions lead to c-Abl activation (Brasher and Van Etten, 2000; Mayer and Baltimore, 1994; Brasher et al., 2001; Hantschel et al., 2003). Furthermore, mutations inside the myristoyl binding site that introduce bulky or polar groups lead to c-Abl activation, presumably by affecting the binding of the N-terminal myristoyl group to this site (Hantschel et al., 2003). N-terminal deletion through gene fusion results in the constitutively active Bcr-Abl protein which is the driver oncoprotein for the development of chronic myelogenous leukemia (CML).

Since aberrant kinase activation is involved in many disease states, especially in the onset and development of cancer, kinase inhibition has been an active area of research for developing new therapeutics. Although less effort has been devoted to the development of kinase activators compared to ATP-binding inhibitors, some examples can be found in a recent review (Simpson et al., 2009). It is becoming clearer that specific kinase activators can not only serve as important tools for enhancing our understanding of kinase regulation, but also have therapeutic applications in a growing number of diseases. Recent publications suggest a role of c-Abl activation in inhibiting mammary tumorigenesis and breast cancer cell mobility and invasiveness (Allington et al., 2009; Noren et al., 2006). c-Abl activation also has potential applications in treating neutropenia since it has been suggested that c-Abl is critical in maintaining normal myelopoiesis (Caracciolo et al., 1989; Rosti et al., 1995). Therefore, we have selected c-Abl 1b (henceforth referred to as c-Abl) as a model system for a kinase activator screening effort. The goal of this exercise was to identify cell-permeable, small-molecule tool compounds that potently activate c-Abl kinase activity both in vitro and in the cell. These specific c-Abl kinase activators will enable further analyses of the complex c-Abl biology, especially of how activation of c-Abl differentiates functionally from the constitutively active Bcr-Abl.

Through this work, we have identified a small-molecule, DPH, that binds to the myristoyl binding site and leads to activation of c-Abl kinase activity. This molecule also demonstrates robust cellular activity in stimulating the phosphorylation of c-Abl and its downstream substrate, Crk. The crystal structure of this activator with the c-Abl kinase domain suggests a potential mechanism of activation that is consistent with the proposed model. The significance and implications of this finding, along with a recently published small-molecule c-Abl inhibitor (GNF-2) that binds to the same myristoyl binding site (Zhang et al., 2010; Adrian et al., 2006), are discussed.

RESULTS

Discovery of c-Abl Activator, DPH

A high-throughput screening (HTS) campaign against the GlaxoSmithKline (GSK) internal compound library was carried out to identify c-Abl activators (Cottom et al., 2011). Unlike in vivo, c-Abl can be activated in the presence of ATP alone, although at a very slow rate, in vitro. Therefore, the screening was designed to look for small molecules that could further enhance the rate of c-Abl activation in the presence of ATP. The N-terminal catalytic domain of c-Abl enzyme used in this screening (c-Abl$^{1-531}$) has been shown to be in its inactive state and is fully activatable (see Figure S1A available online), hence suitable for activator screening.

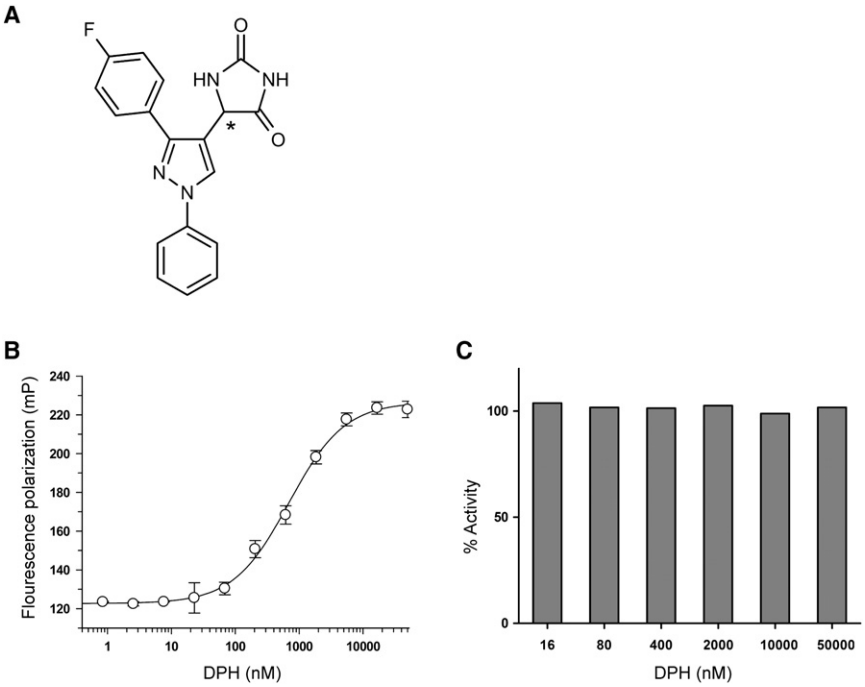

Figure 2. Effect of DPH on c-Abl Activation and Kinase Activity

(A) Structure of DPH. The chiral center is represented by an asterisk (*).

(B) Effect of DPH on c-Abl$^{1-531}$ activation in the end point c-Abl activation assay (Cottom et al., 2011). A 3-fold dilution of DPH was carried out in DMSO with a top concentration of 50 μM. The c-Abl activation reactions were carried out as described (Cottom et al., 2011) in the presence of various concentrations of DPH. A pEC_{50} of 6.1 ± 0.03 is obtained from data fitting which corresponds to an EC_{50} of 794 nM. Data are represented as mean ± SD.

(C) Kinase activity of fully activated c-Abl was measured in the presence of various concentrations of DPH (50, 10, 2, 0.4, 0.08, and 0.016 μM) in a filter binding activity assay (Cottom et al., 2011). % activity = percentage of kinase activity in the presence of DPH relative to the control activity that was measured in the absence of DPH which was set as 100%.

See also Figure S1.

Two in vitro c-Abl activation assays were employed for the characterization of c-Abl activators: an end-point activation assay (IMAP) used in HTS, and a continuous activation assay (Omnia) described in the next section. The end-point IMAP assay is a two-step assay. In this assay, c-Abl is first activated in the presence of ATP and a small-molecule compound for 10 min. A peptide substrate is then added to measure the c-Abl kinase activity acquired in the first step (Cottom et al., 2011).

DPH (5-[3-(4-fluorophenyl)-1-phenyl-1H-pyrazol-4-yl]-2,4-imidazolidinedione or 5-(1,3-diaryl-1H-pyrazol-4-yl)hydantoin) (Figure 2A) was identified as a c-Abl activator from HTS. A dose-response analysis of DPH in the end-point activation assay (IMAP) using the inactive c-Abl$^{1-531}$ gave a pEC_{50} of 6.1 ± 0.03 (EC_{50} = 794 nM) (Figure 2B). DPH also stimulates in vitro c-Abl phosphorylation (Figure S1B).

Further Characterization of the Activation Effect of DPH

Since the end-point activation assay contains both c-Abl activation and activity steps, activation by DPH could be a result of the compound effect on c-Abl activation, its kinase activity, or both. To further dissect the mechanism of activation by DPH, high concentrations of c-Abl$^{1-531}$ (2 μM) and ATP (500 μM) were incubated for 1 hr to preactivate c-Abl$^{1-531}$ and its activity was then measured in the presence of DPH. Since c-Abl was fully activated, this reaction only measured the effect of DPH on the kinase activity of c-Abl. As shown in Figure 2C, DPH has no effect on the kinase activity of c-Abl within the same concentration range used in Figure 2B. This study indicates that DPH acts through stimulating c-Abl activation, rather than its kinase activity.

One limitation of the end-point activation assay is that the selection of assay end-point could affect the activator potency measured from the assay (Kenakin, 2006). In order to determine the true potency of DPH, the continuous activation assay (Omnia) was employed. This assay utilizes an Omnia peptide that emits fluorescence upon phosphorylation (Shults et al., 2006), allowing the continuous monitoring of c-Abl kinase activity during its activation. This analysis takes into consideration the entire activation progress curve, therefore avoiding errors introduced by taking arbitrary assay end-points. As expected, when preactivated c-Abl$^{1-531}$ kinase was used in this assay, a linear reaction progress curve was observed since the reaction rate did not change over time (Figure 3A). However, unactivated c-Abl$^{1-531}$, when used in this reaction, was gradually activated which resulted in a curvilinear reaction progress curve (Figure 3A). This progress curve contains the initial phase (inactivated), the transition phase (partially activated) and the final phase (fully activated). The relaxation time (τ) is defined by the rate at which the reaction transitions from the initial to the final phase. When DPH was titrated in this reaction, an activation effect was observed by a dose-dependent shortening of the relaxation time, indicating a faster rate of c-Abl activation (Figures 3A and 3B). The relaxation time at infinite DPH concentration (τ_{min}) was obtained by plotting the relaxation time against the DPH concentration and fitting the data to Equation 3 (Figure 3B). Since the τ_{min} value was fitted by extrapolating [DPH] to infinity in which the full potency of DPH is realized, the 4-fold activation determined in this analysis $[(\tau_{max} - \tau_{min})/\tau_{min}]$ represents the intrinsic activation capacity of DPH.

DPH Binds to the Myristoyl Binding Site of c-Abl

Based on the crystal structure, the N-terminal myristoyl group of c-Abl binds to the myristoyl binding site on the C-lobe of the kinase domain and this binding helps maintain the inactive conformation of c-Abl (Figure 1). To determine if DPH induces c-Abl activation by binding to the myristoyl binding site to

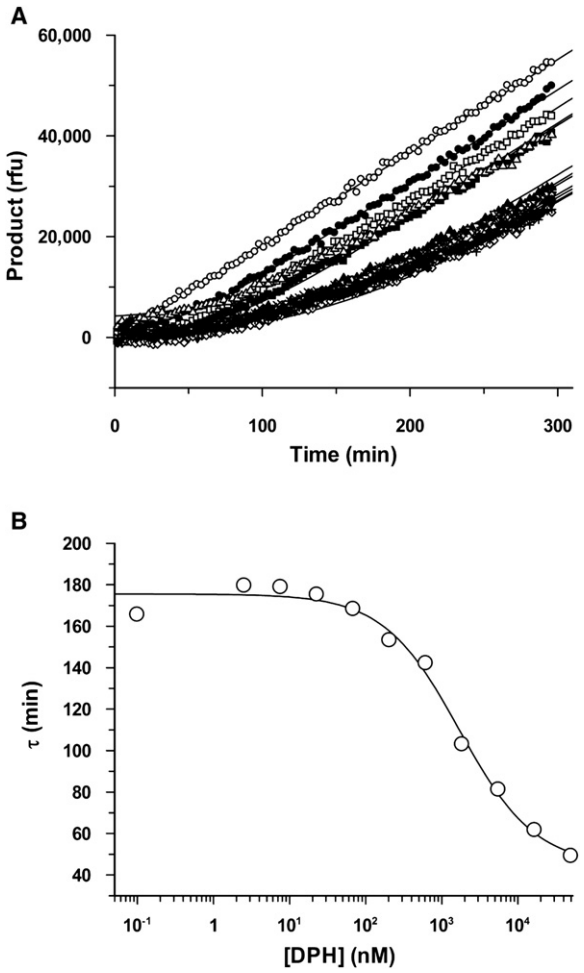

Figure 3. Determination of the Intrinsic Activation Potency of DPH in the Continuous c-Abl Activation Assay

(A) Progress curve analysis of c-Abl$^{1-531}$ activation in the presence of DPH. In this analysis, DPH and unactivated c-Abl were mixed in the presence of 50 μM ATP and 26 μM Omnia peptide. The reaction progress curves were monitored at various DPH concentrations (x, 0; +, 2.5; ◆, 7.6; ◇, 23; ▼, 69; ▽, 206; ▲, 617; Δ, 1852; ■, 5556; □, 16,667; ●, 50,000 nM). Solid lines represent fitting of the data to Equation 1. A preactivated c-Abl was included as a control (○) which gave a linear reaction progress curve. From this analysis, the relaxation time (τ) of c-Abl activation was determined by Equation 2 at each DPH concentration.

(B) The relaxation time was plotted against DPH concentration and fitted to Equation 3 to generate a 4-fold intrinsic activation activity of DPH. The EC_{50} determined in this assay does not reflect the true binding affinity between the activator and the enzyme since this parameter is also affected by the kinetics of the c-Abl autoactivation reaction.

displace the terminal myristoyl group, a fluorescence polarization (FP) competition binding assay was utilized.

This assay used a kinase-dead, N-terminal truncated c-Abl$^{46-534}$ (D382N) and a TAMRA-labeled peptide ligand that bears the same sequence as c-Abl 1b N terminus (underlined) with a myristoyl group (Myr-GQQPGKVLGDQRRPSL(K-TAMRA) G-amide; Myr: myristoyl group). Truncation of the N terminus of c-Abl produces an empty myristoyl pocket for peptide ligand and small-molecule binding. The kinase-dead mutation prevents

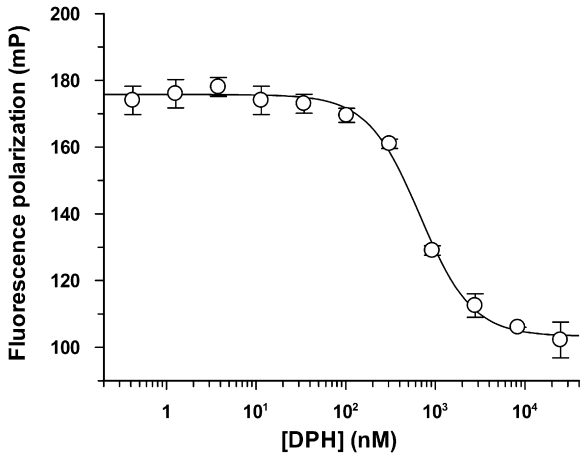

Figure 4. DPH Displaces the Peptide Ligand from the Myristoyl Binding Site in the Fluorescence Polarization Assay

The reactions were carried out in the presence of 160 nM c-Abl$^{46-534}$ (D382N), 30 nM peptide ligand and various concentrations of DPH (25 μM top concentration, 3-fold dilution). The binding K_d from this analysis is 137 ± 7 nM. Data are represented as mean ± SD. See also Figure S2.

protein phosphorylation and enables the generation of a more homogeneous protein prep. Binding of the peptide ligand to the myristoyl site of c-Abl can compete with small molecules that also bind to this site. The displacement of the peptide ligand leads to a change in fluorescence anisotropy which can be used to calculate the binding affinity of the small molecules.

The binding of the peptide ligand to c-Abl was confirmed in the FP binding experiment with a binding K_d of 38 nM (Figure S2A). When a control peptide with an identical amino acid sequence to that of the ligand peptide, but lacking the myristoyl group, was used in the binding assay, no anisotropy change was observed (Figure S2B), indicating that the binding is specific and requires the presence of the myristoyl group. When ATP was used in the assay, no competition with the peptide ligand was observed, indicating that the peptide ligand does not bind to the ATP pocket (Figure S2C). These data, taken together, strongly suggest that the peptide ligand binds specifically to the myristoyl binding site on c-Abl.

When DPH was tested in the FP competition binding assay, a clear dose-response effect was observed with a fitted K_d of 137 ± 7 nM (Figure 4). These data indicate that DPH interacts with c-Abl in the myristoyl binding site. DPH is a racemic mixture of two enantiomers. When these two enantiomers were separated and tested individually in the FP binding assay and the end-point c-Abl activation assay, they displayed different activities. One enantiomer was active in both assays with a binding pIC_{50} of 6.4 (IC_{50} = 398 nM) and activation pEC_{50} of 6.6 (EC_{50} = 251 nM), whereas the other lost ~20-fold activity in both assays (a binding pIC_{50} of 5.1 and activation pEC_{50} of 5.3). These results suggest that a specific configuration of DPH is required for its binding to the myristoyl binding pocket.

Cocrystal Structure of DPH with the c-Abl Kinase Domain

The above FP binding data strongly suggest that DPH binds to the myristoyl binding site of c-Abl. To gain a better

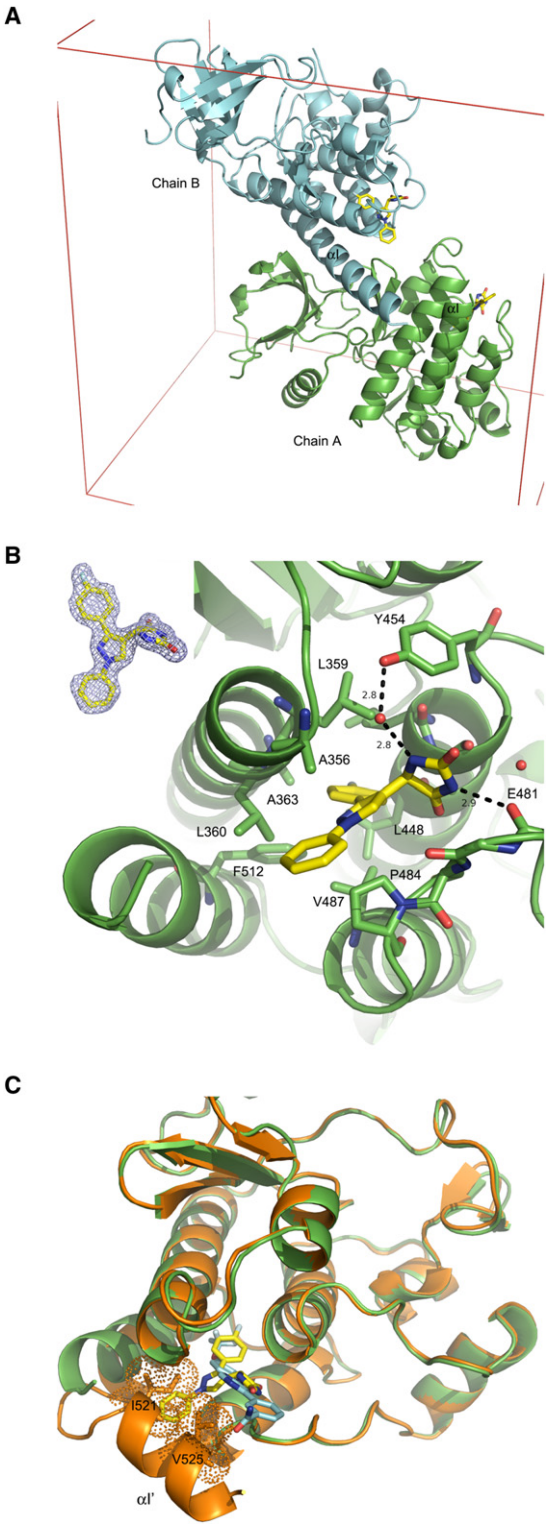

Figure 5. The Cocrystal Structure of *R*-DPH and the c-Abl$^{248-531}$

(A) Packing of crystal asymmetric unit. Chain B (cyan) shows a longer αI helix ending at residue 529 and packing against chain A (green). The αI helix for chain A is only visible to residue 519. The remaining residues, 520–531, are disordered and not visible. DPH is rendered as yellow sticks for carbon, red for oxygen, blue for nitrogen, and white for fluorine.

(B) Interactions of *R*-DPH (yellow) and the c-Abl myristoyl site. Key amino acid residues are rendered as sticks with labels. Key hydrogen bonding interactions are indicated with dashed lines and are annotated with distances (Å). 2-NH hydrogen bonds to a water molecule and 4-NH hydrogen bonds to E481. Figure inset (upper left) shows the electron density for *R*-DPH.

(C) Overlay of the cocrystal structures of *R*-DPH (yellow) and GNF-2 (cyan, PDB code 3K5V) bound to the c-Abl kinase C-lobe domains (green and orange, respectively). The dots represent the Van der Waals surface of I521 and V525 to illustrate the overlap with the space occupied by the phenyl group of DPH.

understanding of the molecular interactions that govern the binding, a cocrystal structure of the more active enantiomer of DPH with the c-Abl kinase domain spanning residues 248 to 531 (c-Abl$^{248-531}$) was obtained. Crystals diffracted to 1.85 Å resolution with space group $P2_12_12_1$ and cell parameters of a = 74.39 Å, b = 95.43 Å, and c = 115.50 Å and two molecules in the asymmetric unit (Figure 5A and Table 1). The crystal structure (Figure 5B) shows that the more active enantiomer has *R* configuration and thus is referred to as *R*-DPH. *R*-DPH binds to c-Abl in the myristoyl binding site and straightens the αI' helix to elongate the αI helix (Figure 5A). In chain A, the αI helix extends to residue 519 and in Chain B, the αI helix extends to residue 529. The remaining C-terminal residues of the respective molecules in the asymmetric unit are disordered. In contrast, the autoinhibited c-Abl has αI helix ending at residue 515, with a loop between residues 515–521 and with αI' helix defined by residues 521–529 (Figure 1). The elongated αI helix of Chain B with *R*-DPH shows significant crystal packing and is an artifact of crystallization. However, the C terminus of Chain A with *R*-DPH shows no crystal packing and will be the focus of subsequent discussion.

The fluorophenyl ring of *R*-DPH occupies a hydrophobic pocket defined by Leu359, Leu360, Ala363, Val487, Leu448, and Phe512 (Figure 5B). The 2-NH of the hydantoin ring of *R*-DPH is hydrogen-bonded to the side chain of Tyr454 via a mediating water molecule, while the 4-NH of the hydantoin forms a direct hydrogen bond with the backbone carbonyl group of Glu481. The pyrazole core of *R*-DPH has Van der Waals contacts with Pro484. The phenyl ring extends toward the elongated αI helix and sits in a lipophilic groove with Ala356 and Pro484 defining respective walls of the groove. One edge of the phenyl ring is solvent exposed.

Contrary to what is seen with the *R*-DPH bound structure where the αI helix is in the extended conformation, c-Abl with GNF-2 (Zhang et al., 2010) shows that the αI helix stops at Phe516 and the αI' helix defined by residues 521–529 packs against GNF-2, similar to what is seen in the myristoyl-bound autoinhibited c-Abl structure (Figure 1). An overlay of the *R*-DPH structure with the GNF-2 bound c-Abl structure illustrates the significant conformational differences in the αI and αI' helices (Figure 5C). The phenyl ring of *R*-DPH occupies space where αI' helix would reside in the inhibited form of c-Abl with GNF-2. These structural differences provide the basis for the opposing effects of GNF-2 and DPH on c-Abl activity.

DPH Is Cell Permeable and Stimulates Full-Length c-Abl Activation in HEK-MSRII Cells

So far, our data have demonstrated that DPH is a potent activator of N-terminal kinase domain (1-531) of c-Abl in vitro.

Table 1. Data Collection and Refinement Statistics for the Cocrystal Structure of *R*-DPH and c-Abl$^{248-531}$

	R-DPH w/ c-Abl Kinase Domain
Data collection	
Space group	$P2_12_12_1$
Cell dimensions	
a, *b*, *c* (Å)	74.39, 95.43, 115.50
α, β, γ (°)	90, 90, 90
Resolution (Å)	30–1.85 (1.9–1.85)[a]
R_{sym} or R_{merge}	0.048 (0.502)
$I / \sigma I$	41 (2.7)
Completeness (%)	99 (98.3)
Redundancy	5 (4.9)
Refinement	
Resolution (Å)	30–1.85
No. reflections	66950
R_{work} / R_{free}	0.189/0.204
No. atoms	
Protein	4250
Ligand/ion	160
Water	215
B factors	
Protein	33.9
Ligand/ion	35.6
Water	33.7
Rmsd	
Bond lengths (Å)	0.007
Bond angles (°)	1.076

[a] Values in parentheses are for highest resolution shell.

To determine if DPH is cell-permeable and if it can activate full-length c-Abl in the cell, the cellular effect of DPH was determined by measuring the phosphorylation status of Y245 and Y412 of c-Abl upon DPH treatment as a surrogate for c-Abl activation in cells. Such c-Abl phosphorylation can be induced by pervanadate or growth factor treatments. However, in our hands, commercially available pY412 and pY245 antibodies were insensitive in detecting DPH-stimulated endogenous c-Abl phosphorylation by western blot (Figure 6A, lanes 1–4, and Figure 6B, lane 1). We hypothesize that the c-Abl phosphorylation is milder with DPH, than with more strenuous treatments, such as pervanadate or growth factor treatments, that may be inducing multiple pathways of activation of c-Abl. To overcome this difficulty, we overexpressed human c-Abl 1b (full length) in HEK-MSRII cells by BacMam transduction (Cottom et al., 2011), which improved western blot detection of pY245 and pY412 c-Abl in cell lysates. As shown in Figures 6A and 6B, DPH induced both pY245 and pY412 c-Abl phosphorylation. In addition to pY245 and pY412 bands, these antibodies detected many nonspecific bands which were also induced by DPH treatment. Interestingly, the inductions of specific, as well as nonspecific, bands in response to DPH treatment were completely abrogated by imatinib (Figure 6A), suggesting that the nonspecific bands may be either substrates or breakdown products of c-Abl. To further confirm the effect of DPH on Y412 phosphorylation, we immunoprecipitated c-Abl from cells treated with DPH or DMSO and determined the change in Y412 phosphorylation upon treatment with DPH by mass spectrometric analysis. A 2.5- to 3-fold increase in Y412 phosphorylation by DPH (10 μM) treatment (apparent phosphorylation stoichiometry ~55%), as compared with cells treated with DMSO (apparent phosphorylation stoichiometry ~20%) was observed. The cellular EC_{50} of DPH on Y245 phosphorylation was determined to be 2.5 μM (pEC_{50} = 5.6 ± 0.2) in HEK-MSRII cells by InCell western assay (Figure 6C). Taken together, these data strongly indicate that DPH is cell-permeable and can activate full-length c-Abl in cells.

DPH Induces the Phosphorylation of c-Abl Substrate Crk

In the above work, we demonstrated that Y245 and Y412 phosphorylation was induced upon treating the cells with DPH. To test if DPH was able to activate endogenous c-Abl in cells, we measured the phosphorylation of c-Abl substrate, Crk, in cells that were treated with DPH. Crk is a well-characterized cellular substrate of c-Abl. It is phosphorylated by active c-Abl. The pCrk antibody we utilized recognizes pY221 of Crk and pY207 of Crk-L, a Crk isoform. We first treated KG-1, a human myeloid cell line, with DPH and detected Crk-L pY207 by immunoblotting as a readout for enhanced c-Abl kinase activity. In accordance to our hypothesis, DPH induction of Crk-L pY207 in KG-1 cells was dose dependent. Moreover, these inductions were completely abolished by imatinib treatment, suggesting a dependence on the c-Abl kinase activity (Figure 6D). We also developed a western blot pCrk (pY221) assay for the detection of endogenous c-Abl activation in HepG2 cell line. Consistent with c-Abl pY245 InCell western analysis, a cellular EC_{50} of DPH of 2.5 μM (pEC_{50} = 5.6 ± 0.2) was also observed in the HepG2 pCrk assay (Figure 6E**)**. These results confirmed DPH as a cell-permeable small-molecule activator of c-Abl.

DISCUSSION

In this paper, we describe a small-molecule activator (DPH) of the c-Abl kinase that was identified through HTS of a ~1.3 million compound library. We show that this molecule demonstrates both enzymatic and cellular c-Abl activation activities. It stimulates phosphorylation of c-Abl and only affects the activation process of c-Abl with no effect on its kinase activity. Structural studies demonstrate the binding of this small-molecule to the myristoyl binding site and suggest a potential mechanism of c-Abl activation by DPH.

c-Abl activation is an extremely dynamic process marked by the disassembly of the compact autoinhibited conformation, followed by the phosphorylation of two key Tyr residues (Y245 and Y412). Based on structural data, the autoinhibited conformation of c-Abl is maintained through the binding of the N-terminal myristoyl group to the myristoyl binding site on the kinase domain. This event provides specific intramolecular interactions for the formation of the bent conformation of the αI helix which is required for the docking of the SH2 domain onto the kinase domain. These interactions appear to be mainly provided by the myristoyl group with minimal contributions from the adjacent tether peptide sequence, as a bent conformation of the αI helix is

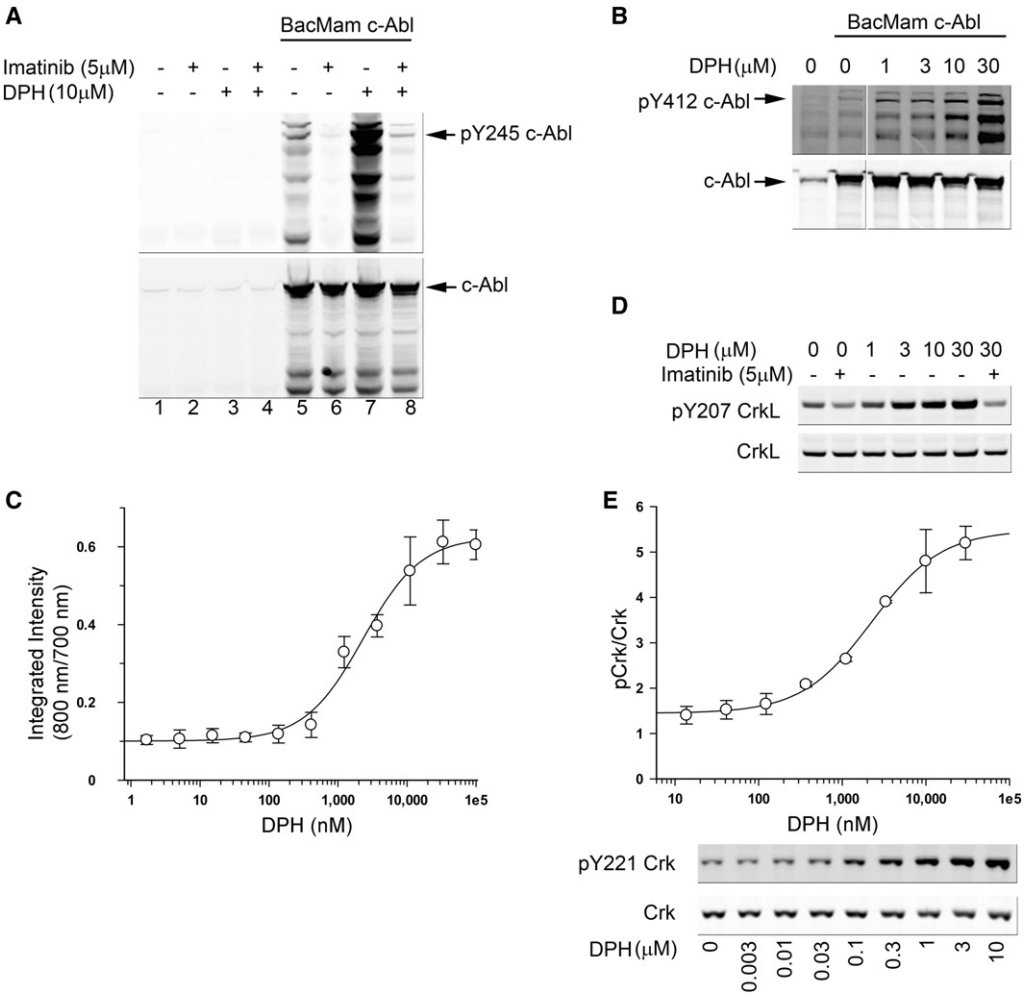

Figure 6. DPH Activates c-Abl in Cells

(A) (B) DPH-induced phosphorylation of c-Abl Y245 (A) and Y412 (B). Immunoblots show the inductions in phosphorylation (pY245 and pY412) by DPH in HEK-MSRII cells transduced with c-Abl. Imatinib inhibits Y245 phosphorylation induced by DPH.

(C) Dose response analysis of DPH on Y245 phosphorylation in HEK-MSRII cells transduced with c-Abl by InCell western assay (Cottom et al., 2011) gave a cellular EC_{50} of 2.5 μM (pEC_{50} = 5.6 ± 0.2). The integrated intensity (800/700 nm) was calculated as described elsewhere (Cottom et al., 2011). Data are represented as mean ± SD.

(D) Imatinib-sensitive dose-dependent induction of pY207 Crk-L in KG-1 cells treated with DPH.

(E) Dose-dependent induction in pY221 Crk in DPH-treated HepG2 cells by western blot analysis. Ratios of pixel intensities of pY221 Crk/total Crk in DPH treated to DMSO control derived from the western blot was fitted in a nonlinear curve graph to give a cellular EC_{50} of 2.5 μM (pEC_{50} = 5.6 ± 0.2). Data are represented as mean ± SD.

induced in the crystal structure of c-Abl$^{46-534}$ with myristic acid added in *trans* (Nagar et al., 2003).

In principle, it is possible to find small molecules that bind to the myristoyl binding site and provide molecular interactions that either stabilize or destabilize the bent conformation of the αI helix. Such molecules are expected to significantly affect the c-Abl activation process. The identification of DPH from HTS provided a unique opportunity for the study of c-Abl activation mechanism. The site of interaction of this molecule with c-Abl was mapped to the myristoyl binding site by both competition binding and crystallographic studies. Furthermore, detailed structural analyses suggest a potential mechanism of activation by this molecule. The overlay of the structure of inactive c-Abl with the structure of the c-Abl kinase domain bound to *R*-DPH identifies steric clashes between the left hand side phenyl moiety of *R*-DPH and the αI' helix. These clashes can be clearly seen as the phenyl moiety extending into the Van der Waals surface of the αI' helix, indicating that *R*-DPH is too bulky for αI helix to adopt the bent conformation (Figure 5C). As described above, the bent conformation of the C-terminal helix to form αI' provides a necessary platform for the docking of the SH2 domain and formation of the autoinhibited c-Abl conformation. Inability to form this bent conformation therefore leads to c-Abl activation. During the preparation of this manuscript, we encountered one recent publication from a different group on the identification of small-molecule myristoyl site-binding c-Abl activators through a NMR-based fragment screening (Jahnke et al., 2010). Further structural analysis indicated that the binding of these molecules

to the myristoyl site prevented the αI helix from forming the bent conformation. These results are in full agreement with our data and further validate the mechanism of action of this type of c-Abl activators. However, DPH differs from these activators in two important ways. The published c-Abl activators have weak (micromolar) potency and show no cellular activity. In contrast, DPH is more potent (with nanomolar potency), cell-permeable and demonstrates robust cellular c-Abl activation activity. To our knowledge, there are currently no cell-permeable tool compounds available for c-Abl activation. Therefore, DPH represents the first such tool compound with immediate applications in the study of in vivo c-Abl biology.

While compounds binding to the enzyme active site almost invariably act as inhibitors simply by competing with the substrate, allosteric binders can elicit differential responses depending on the specific molecular interactions they induce. Recently, a small-molecule inhibitor of c-Abl, GNF-2, was identified that also binds to the myristoyl binding site (Adrian et al., 2006; Zhang et al., 2010). This molecule is structurally distinct from DPH. Analysis based on the c-Abl/GNF-2 cocrystal structure suggests that GNF-2 interacts closely with the αI' helix and stabilizes its bent conformation (Figure 5C). Therefore, one potential mechanism of GNF-2 inhibition could be its stabilization of the autoinhibited c-Abl conformation. Such interaction complements the function of the myristoyl group, especially in the event that the N-terminal myristoyl group spontaneously dissociate from the myristoyl binding pocket (Zhou, 2003).

Based on these observations, the following model can be proposed to predict the effect of small-molecule modulators that bind to the myristoyl pocket of c-Abl. The compound is inhibitory if it stabilizes the bent conformation of the αI helix. It is activating if it disrupts such bent conformation. Certain compounds may bind in a way that neither disrupt nor reinforce the bent conformation of the αI helix. These compounds act merely as displacers of the myristoyl group and by doing so, eliminate the stabilizing interactions on the bent conformation of the αI helix induced by myristoyl group binding. Therefore, such compounds are predicted to also act as c-Abl activators. We have observed compounds of this nature in our lead optimization efforts and the results will be presented elsewhere.

In vivo, protein conformational states are stabilized/destabilized not only by intramolecular forces, but also by interactions with various ligands and protein partners. For example, strong experimental evidence suggests that apart from the autoinhibition mechanism described so far in this paper, c-Abl inactive state is likely also maintained by cellular binding proteins that stabilize this autoinhibited conformation (Wang, 2004). This complicates the study on c-Abl regulation because for the most part, the nature of these proteins and their interactions with c-Abl are unknown. However, it is likely that a small-molecule activator identified in the in vitro setting could, given sufficient potency, tip the balance between the active/inactive states of c-Abl in vivo, trigger its autoactivation cycle, and eventually lead to c-Abl activation. In support of this hypothesis, we saw robust cellular c-Abl activation and Crk phosphorylation upon DPH treatment. This potent cellular activity of DPH enables further investigation of the roles of c-Abl in processes such as myelopoiesis, tumorigenesis and DNA damage responses.

SIGNIFICANCE

Although some progress has been made in understanding the biochemical mechanism of c-Abl kinase activation and identification of its cellular substrates, phenotypic outcomes of c-Abl kinase activation in vivo remain elusive due to the lack of a viable method to activate endogenous c-Abl function. Recently, it was suggested that the activation of c-Abl/Crk pathway inhibits mammary tumorigenesis, invasion, and metastasis (Allington et al., 2009; Noren et al., 2006). It was also suggested that c-Abl is critical for the normal myelopoiesis process (Caracciolo et al., 1989; Rosti et al., 1995). Therefore, development of small-molecule c-Abl activators allows further investigation of the physiological as well as pathophysiological functions of endogenous c-Abl. In this report, we identified a potent cell-permeable c-Abl activator, DPH, that binds to the myristoyl binding pocket of c-Abl, prevents the bending of the αI helix and docking of the SH2 domain, and induces c-Abl activation. Hence, the mode of action of DPH confirms the previously hypothesized mechanism for c-Abl activation (Nagar et al., 2003, 2006). We showed that, in addition to its in vitro activity, DPH also demonstrates robust cellular activity in c-Abl activation. Therefore, the identification of DPH provides a valuable tool molecule for the study of the functions of endogenous c-Abl in a multitude of biological processes.

EXPERIMENTAL PROCEDURES

Peptides used in the FP assay were custom synthesized by 21st Century Biochemicals, LLC. Omnia peptide (Ac-KKGEAIYAAdP(Sox)G-NH2) was purchased from Invitrogen (Omnia Y Peptide 6, Catalog # KNZ3061) (Shults et al., 2006). All peptides were greater than 95% pure. Their identity was confirmed by mass spectrometric analysis. All other reagents are of analytical grade or higher.

Cloning, Expression, and Purification of c-Abl$^{1-531}$, c-Abl$^{46-534}$ (D382N) and c-Abl$^{248-531}$ (kinase domain)

The full-length c-Abl Ib cDNA (GenBank NM_007313) was generated by PCR and cloned into pENTR/D-TOPO cloning vector as described by manufacturer (Invitrogen Inc.). Cloning, expression, and purification of c-Abl$^{1-531}$ has been described elsewhere (Cottom et al., 2011). Cloning, expression, and purification of c-Abl$^{46-534}$ (D382N) and c-Abl$^{248-531}$ were described in the Supplemental Experimental Procedures.

Continuous c-Abl Activation Assay

c-Abl activation was monitored continuously in a reaction mix containing ATP (50 μM), the Omnia peptide and various concentrations of DPH (concentrations indicated in text and/or figure legend) in 50 mM MOPS (pH 7.2), 2 mM $MgCl_2$, 1 mM DTT, 0.1 mg/ml BSA, 0.01% Tween-20, and 25 mM NaCl. For the control experiment, c-Abl$^{1-531}$ (2 μM) was preactivated by incubating with 500 μM ATP for 1 hr at room temperature. To initiate the activation reactions, c-Abl$^{1-531}$ was added at a concentration of 0.5 nM with a final reaction volume of 20 μl. The reactions were run in a black 384 well plate (Corning Costar #3658) and the product formation was monitored by a continuous fluorescence detection assay (Omnia assay, Invitrogen). Phosphorylation of the Omnia peptide was quantified using an Envision 2102 fluorescence plate reader (PerkinElmer) with an excitation and emission wavelength of 380 and 486 nm, respectively.

The c-Abl activation progress curves were fitted in Equation 1 describing intermolecular enzyme activation during catalysis (Wu and Wang, 2003) for the determination of the activation rate constant, k_{obs}, which was further converted to the relaxation time, τ, by Equation 2 (Wu and Wang, 2003).

$$P = \frac{C}{k}\ln\{1 - \alpha(1 - e^{k_{obs}Et})\} + b \quad (1)$$

$$\tau = \frac{\ln \alpha}{(\alpha - 1)k_{obs}E} \quad (2)$$

In above equations, P is the amount of product, C is the specific activity of fully activated c-Abl determined experimentally, k_{obs} is the transition rate constant, α is the fraction of active c-Abl at t = 0 (calculated as a ratio between the basal activity and the full activity), E is total c-Abl concentration, t is time and b is background.

The τ values thus determined were then plotted against DPH concentrations and the data were fitted to a general 4-parameter EC_{50} equation (Equation 3) to generate τ_{max}, τ_{min}, Hill coefficient (h) and the EC_{50} values. In this equation, τ_{max} and τ_{min} represent maximum and minimum value of τ, respectively, and [A] is DPH concentration.

The fold of activation was calculated, fold of activation = $(\tau_{max} - \tau_{min})/\tau_{min}$.

$$\tau = \tau_{min} + \left((\tau_{max} - \tau_{min})/\left(1 + ([A]/EC_{50})^{h}\right)\right) \quad (3)$$

c-Abl Phosphorylation Gel Analysis

Total phosphorylation of c-Abl during activation was monitored by the incorporation of the ^{33}P radiolabel onto the protein during the activation reactions with [γ-^{33}P]ATP (10 mCi/ml, PerkinElmer). The c-Abl$^{1-531}$ activation reactions were carried out as described above in the presence or absence of DPH and quenched at various times by the addition of the SDS-PAGE sample loading buffer. Quenched samples were analyzed by SDS-PAGE and the amount of ^{33}P incorporation in c-Abl was quantified by Phosphoimager (Storm, MolecularDynamics).

Fluorescence Polarization Binding Assay

The FP binding assay was carried out in pH 7.2, 20 mM MOPS buffer containing 10 mM $MgCl_2$, 2 mM CHAPS, 25 mM NaCl, 0.1% pluronic acid, 0.05 mg/ml BSA, and 1 mM DTT. The final concentration of c-Abl$^{46-534}$ (D382N) and the peptide ligand (Myr-GQQPGKVLGDQRRPSL(K-TAMRA)G-amide) is 160 and 30 nM, respectively. The compound dilution was carried out in DMSO in a 96-well, round-bottom polypropylene plate (Costar Catalog # 3359) and was transferred (0.5 μl/well) to a black, round-bottom 384-well assay plate (Costar catalog # 3658). DMSO (0.5 μl/well) was added for low control (peptide ligand only) and high control (peptide ligand + c-Abl, no compound). Peptide ligand in the above buffer was then added (5 μl/well) to the assay plate, followed by the c-Abl mix (5 μl/well). Plate was vortexed slightly to mix and was allowed to equilibrate for 30 min. Fluorescence anisotropy readout was taken on an EnVision (PerkinElmer) 2102 fluorescence plate reader. The dissociation constant (K_d) was determined using a method described previously (Wang, 1995).

Synthesis and Characterization of DPH

To a solution of 3-(4-fluorophenyl)-1-phenyl-1H-pyrazole-4-carbaldehyde (3 g, 11.27 mmol) and ammonium carbonate (4.33 g, 45.1 mmol) in ethanol (45 ml) and water (45 ml), potassium cyanide (1.467 g, 22.53 mmol) in water (approximately 5 ml) was added and stirred at 70°C under nitrogen overnight. The reaction was cooled in an ice bath, and then 2 M hydrochloric acid (30 ml, 60.0 mmol) was added dropwise to the reaction mixture. The solution was left to stir for 3.5 hr. The mixture was added to EtOAc (200 ml) and extracted with EtOAc. The EtOAc phase was washed with brine (6 × 200 ml). The solvent was evaporated to give the crude material of 5-[3-(4-fluorophenyl)-1-phenyl-1H-pyrazol-4-yl]-2,4-imidazolidinedione as a yellow solid (3.3 g, 87%). Fifty milligrams of the crude material was purified by reverse-phase preparative LCMS to give the title compound (DPH) as a colorless solid (35.6 mg). ^1H NMR (400 MHz, DMSO-d_6): δ 10.85 (br. s., 1H), 8.68 (s, 1H), 8.29 (d, J = 0.8 Hz, 1H), 7.93 (dd, J = 0.9, 8.7 Hz, 2H), 7.79–7.85 (m, 2H), 7.48–7.55 (m, J = 7.6, 8.7 Hz, 2H), 7.28–7.37 (m, 3H), 5.26 (d, J = 0.8 Hz, 1H); ^{13}C NMR (101 MHz, DMSO-d_6): δ 174.6, 162.3 (d, J = 245.1 Hz), 157.0, 150.5, 139.2, 130.2 (d, J = 8.8 Hz), 129.5, 128.7 (d, J = 3.2 Hz), 128.3, 126.6, 118.3, 116.8, 115.5 (d, J = 21.6 Hz), 53.5; ^{19}F NMR (376 MHz, DMSO-d_6): δ −114.1 (proton decoupled); HRMS (m/z): [MH]+ calcd. for C18H14FN4O2, 337.1101; found, 337.1100.

Cocrystal Structure of DPH with c-Abl Kinase Domain (c-Abl$^{248-531}$)

c-Abl$^{248-531}$ was incubated overnight with 1 mM DPH and concentrated to 20 mg/ml in 20 mM Tris-HCl [pH 8.0], 100 mM NaCl, 3 mM DTT, and 5% (v/v) glycerol. Crystals were grown by hanging drop vapor diffusion with 200 nl protein and 200 nl reservoir solution at 4°C. The reservoir solution contained 0.4 M ammonium phosphate. Crystals grew in 1–5 days, were transferred to reservoir solution with 15%–30% glycerol and flash-frozen in liquid nitrogen.

Diffraction data were collected at 100 K using 0.97872 Å radiation at the Advanced Photon Source at LifeScience CAT, beamline 21IDf using a Mar225 CCD detector and then integrated and scaled with HKL2000 (Otwinowski and Minor, 1997). Molecular Replacement solutions were found with PHASER (McCoy et al., 2007) and refinement done with Phenix (Adams et al., 2002). Model building was done with COOT (Emsley and Cowtan, 2004) and figures were made with PyMol (http://pymol.sourceforge.net/).

Stimulation of c-Abl Y245/Y412 Phosphorylation in HEK-MSRII Cells by DPH

HEK-MSRII cells were transduced with BacMam c-Abl 1b virus. 48 hr after transduction the cells were treated with DPH at 1–30 μM concentrations for 10 min. Cells pretreated with 5 μM of Imatinib for 10 min was used to identify whether pY245 induction was depended on c-Abl kinase activity.

Stimulation of Crk-L Y207 Phosphorylation in KG-1 Cells by DPH

KG-1 cells (4 × 10^6) were seeded in 1 ml of culture medium in 1.5 ml microcentrifuge tubes. Cells were incubated in a 37°C water bath for 1 hr and treated with DPH for 4 hr. After incubation, cells were pelleted by centrifugation at 1000 × g for 5 min, washed twice in ice cold PBS, and subjected to cell lysis.

Stimulation of Crk Y221 Phosphorylation in HepG2 Cells by DPH

Cells (1.5 × 10^6) were plated in 60 mm dishes. One day after plating, the cells were treated with DPH for 4 hr. The cells were then washed with ice cold PBS and subjected to cell lysis.

ACCESSION NUMBERS

Coordinates have been deposited in the Protein Data Bank with the accession code 3PYY.

SUPPLEMENTAL INFORMATION

Supplemental Information includes Supplemental Experimental Procedures and two figures and can be found with this article online at doi:10.1016/j.chembiol.2010.12.013.

ACKNOWLEDGMENTS

All authors are current or former employees of GlaxoSmithKline. This work was funded by GlaxoSmithKline.

Received: September 20, 2010
Revised: November 19, 2010
Accepted: December 6, 2010
Published: February 24, 2011

REFERENCES

Adams, P.D., Grosse-Kunstleve, R.W., Hung, L.W., Ioerger, T.R., McCoy, A.J., Moriarty, N.W., Read, R.J., Sacchettini, J.C., Sauter, N.K., and Terwilliger, T.C. (2002). PHENIX: building new software for automated crystallographic structure determination. Acta Crystallogr. D Biol. Crystallogr. *58*, 1948–1954.

Adrian, F.J., Ding, Q., Sim, T., Velentza, A., Sloan, C., Liu, Y., Zhang, G., Hur, W., Ding, S., Manley, P., et al. (2006). Allosteric inhibitors of Bcr-abl-dependent cell proliferation. Nat. Chem. Biol. *2*, 95–102.

Allington, T.M., Galliher-Beckley, A.J., and Schiemann, W.P. (2009). Activated Abl kinase inhibits oncogenic transforming growth factor-beta signaling and tumorigenesis in mammary tumors. FASEB J. *23*, 4231–4243.

Brasher, B.B., and Van Etten, R.A. (2000). c-Abl has high intrinsic tyrosine kinase activity that is stimulated by mutation of the Src homology 3 domain and by autophosphorylation at two distinct regulatory tyrosines. J. Biol. Chem. *275*, 35631–35637.

Brasher, B.B., Roumiantsev, S., and Van Etten, R.A. (2001). Mutational analysis of the regulatory function of the c-Abl Src homology 3 domain. Oncogene *20*, 7744–7752.

Caracciolo, D., Valtieri, M., Venturelli, D., Peschle, C., Gewirtz, A.M., and Calabretta, B. (1989). Lineage-specific requirement of c-abl function in normal hematopoiesis. Science *245*, 1107–1110.

Cottom, J., Hofmann, G., Siegfried, B., Yang, J., Zhang, H., Yi, T., Ho, T.F., Quinn, C., Wang, D., Johanson, K., et al. (2011). Assay development and high throughput screening of small molecular c-Abl kinase activators. J. Biomol. Screen *16*, 53–64.

Emsley, P., and Cowtan, K. (2004). Coot: Model-building tools for molecular graphics. Acta Crystallogr. D Biol. Crystallogr. *60*, 2126–2132.

Hantschel, O., Nagar, B., Guettler, S., Kretzschmar, J., Dorey, K., Kuriyan, J., and Superti-Furga, G. (2003). A myristoyl/phosphotyrosine switch regulates c-Abl. Cell *112*, 845–857.

Jahnke, W., Grotzfeld, R.M., Pelle, X., Strauss, A., Fendrich, G., Cowan-Jacob, S.W., Cotesta, S., Fabbro, D., Furet, P., Mestan, J., and Marzinzik, A.L. (2010). Binding or bending: distinction of allosteric Abl kinase agonists from antagonists by an NMR-based conformational assay. J. Am. Chem. Soc. *132*, 7043–7048.

Kenakin, T.P. (2006). A Pharmacology Primer (New York: Academic Press).

Mayer, B.J., and Baltimore, D. (1994). Mutagenic analysis of the roles of SH2 and SH3 domains in regulation of the Abl tyrosine kinase. Mol. Cell. Biol. *14*, 2883–2894.

McCoy, A.J., Grosse-Kunstleve, R.W., Adams, P.D., Winn, M.D., Storoni, L.C., and Read, R.J. (2007). Phaser crystallographic software. J. Appl. Crystallogr. *40*, 658–674.

Nagar, B., Hantschel, O., Seeliger, M., Davies, J.M., Weis, W.I., Superti-Furga, G., and Kuriyan, J. (2006). Organization of the SH3-SH2 unit in active and inactive forms of the c-Abl tyrosine kinase. Mol. Cell *21*, 787–798.

Nagar, B., Hantschel, O., Young, M.A., Scheffzek, K., Veach, D., Bornmann, W., Clarkson, B., Superti-Furga, G., and Kuriyan, J. (2003). Structural basis for the autoinhibition of c-Abl tyrosine kinase. Cell *112*, 859–871.

Noren, N.K., Foos, G., Hauser, C.A., and Pasquale, E.B. (2006). The EphB4 receptor suppresses breast cancer cell tumorigenicity through an Abl-Crk pathway. Nat. Cell Biol. *8*, 815–825.

Otwinowski, Z., and Minor, W. (1997). Processing of X-ray diffraction data collected in oscillation mode. Methods Enzymol. *276*, 307–326.

Rosti, V., Bergamaschi, G., Lucotti, C., Danova, M., Carlo-Stella, C., Locatelli, F., Tonon, L., Mazzini, G., and Cazzola, M. (1995). Oligodeoxynucleotides antisense to c-abl specifically inhibit entry into S-phase of CD34+ hematopoietic cells and their differentiation to granulocyte-macrophage progenitors. Blood *86*, 3387–3393.

Shtivelman, E., Lifshitz, B., Gale, R.P., Roe, B.A., and Canaani, E. (1986). Alternative splicing of RNAs transcribed from the human abl gene and from the bcr-abl fused gene. Cell *47*, 277–284.

Shults, M.D., Carrico-Moniz, D., and Imperiali, B. (2006). Optimal Sox-based fluorescent chemosensor design for serine/threonine protein kinases. Anal. Biochem. *352*, 198–207.

Simpson, G.L., Hughes, J.A., Washio, Y., and Bertrand, S.M. (2009). Direct small-molecule kinase activation: Novel approaches for a new era of drug discovery. Curr. Opin. Drug Discov. Dev. *12*, 585–596.

Sirvent, A., Benistant, C., and Roche, S. (2008). Cytoplasmic signalling by the c-Abl tyrosine kinase in normal and cancer cells. Biol. Cell *100*, 617–631.

Taagepera, S., McDonald, D., Loeb, J.E., Whitaker, L.L., McElroy, A.K., Wang, J.Y., and Hope, T.J. (1998). Nuclear-cytoplasmic shuttling of C-ABL tyrosine kinase. Proc. Natl. Acad. Sci. USA *95*, 7457–7462.

Van Etten, R.A. (1999). Cycling, stressed-out and nervous: cellular functions of c-Abl. Trends Cell Biol. *9*, 179–186.

Wang, J.Y. (1993). Abl tyrosine kinase in signal transduction and cell-cycle regulation. Curr. Opin. Genet. Dev. *3*, 35–43.

Wang, J.Y.J. (2004). Controlling Abl: auto-inhibition and co-inhibition? Nat. Cell Biol. *6*, 3–7.

Wang, Z.X. (1995). An exact mathematical expression for describing competitive binding of two different ligands to a protein molecule. FEBS Lett. *360*, 111–114.

Williams, J.C., Weijland, A., Gonfloni, S., Thompson, A., Courtneidge, S.A., Superti-Furga, G., and Wierenga, R.K. (1997). The 2.35 A crystal structure of the inactivated form of chicken Src: a dynamic molecule with multiple regulatory interactions. J. Mol. Biol. *274*, 757–775.

Wu, H., and Wang, Z.X. (2003). The mechanism of p21-activated kinase 2 autoactivation. J. Biol. Chem. *278*, 41768–41778.

Xu, W., Harrison, S.C., and Eck, M.J. (1997). Three-dimensional structure of the tyrosine kinase c-Src. Nature *385*, 595–602.

Zhang, J., Adrian, F.J., Jahnke, W., Cowan-Jacob, S.W., Li, A.G., Iacob, R.E., Sim, T., Powers, J., Dierks, C., Sun, F., et al. (2010). Targeting Bcr-Abl by combining allosteric with ATP-binding-site inhibitors. Nature *463*, 501–506.

Zhou, H.X. (2003). How often does the myristoylated N-terminal latch of c-Abl come off? FEBS Lett. *552*, 160–162.

